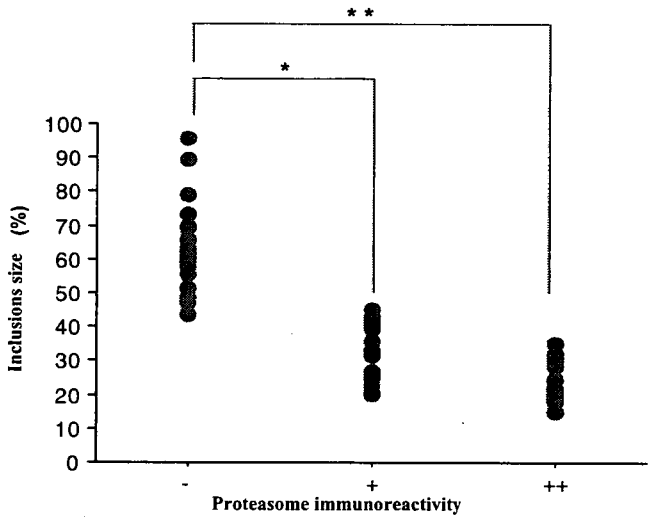

Fig. 3 The percentage of the neurofilamentous inclusions occupying the cytoplasm in each group. The intensity of proteasome immunoreactivity with the proteasome antibody was classified into three groups: (–), weaker than control level; (+), equivalent to control level; and (++), greater than control level. The neurofilamentous inclusions were larger in the (–) group than in the (+) and (++) groups.

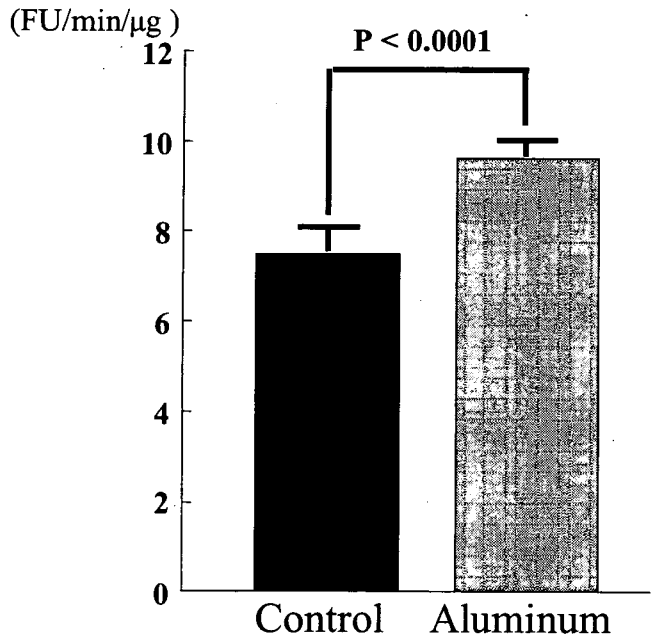

Fig. 4 Proteasome activities in spinal cord extracts from control and aluminum-treated rabbits. The activity was significantly increased in the aluminum-treated rabbits compared to the controls (9.646 ± 0.186 *vs.* 7.510 ± 0.233 FU/min/μg).

neurofilamentous inclusions, in the spinal motor neurons is a common finding in aluminum-treated rabbits,[3,5,7,8,11,12] as well as in patients with amyotrophic lateral sclerosis.[30] In the present study, all experimental rabbits were killed on

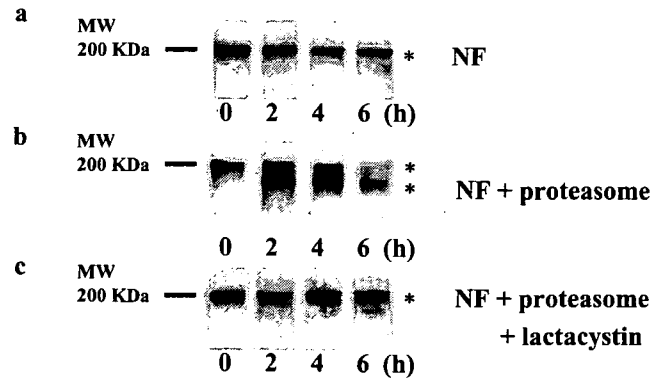

Fig. 5 Western blot analyses of neurofilament-H protein degradation. Incubation of the neurofilament-H protein without the 20S proteasome shows no degradation (a). The neurofilament-H protein is clearly degraded by the 20S proteasome into a 180-kDa band (b). The degradation is significantly inhibited by lactacystin (c). (a) without 20S proteasome; (b) with 100 nM 20S proteasome; (c) with 100 nM 20S proteasome plus 10 μM lactacystin. MW, molecular weight; NF, neurofilament.

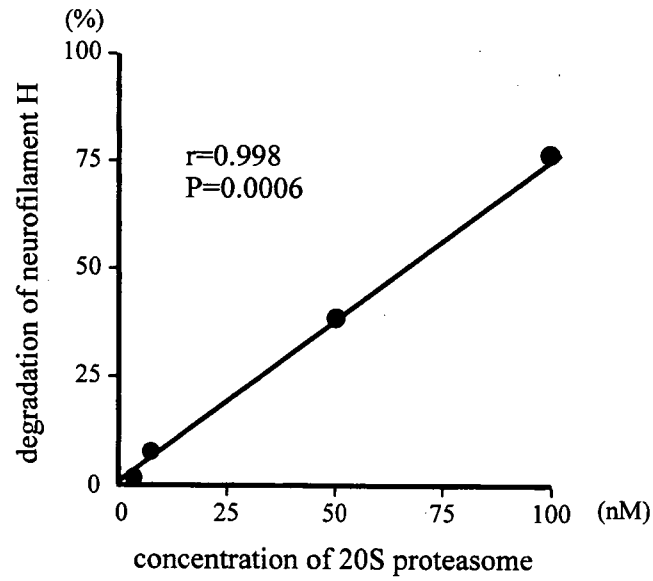

Fig. 6 Degradation of non-phosphorylated neurofilament-H protein at various concentrations (0–100 nM) of the 20S proteasome. The degradation of the neurofilament-H protein closely correlates with the 20S proteasome concentration.

day 7 after the initial injection of aluminum, because previous reports suggested that animals exhibit some neurologic symptoms such as muscle weakness and motor disability within 7 days.[24–26] Our histological study demonstrated that spinal motor neurons from aluminum-treated rabbits developed neurofilamentous inclusions in their cytoplasm, dendrites, and proximal axons. These inclusions showed argentophilia with a modified Bielschowsky stain and intense immunostaining for SMI 31. Thus, we confirmed the occurrence of neurofilamentous inclusions

consisting mainly of phosphorylated neurofilament-H protein, as previously described in models of acute aluminum treatment.[3,7,8,11]

The mechanism underlying the accumulation and phosphorylation of the neurofilament protein is unclear in aluminum-treated rabbits. Some investigators suggested that aluminum modulates apoptosis and inhibits calcium-mediated proteolysis of cytoskeletal proteins via several mechanisms. Aluminum directly inhibits calpain, but only at high concentrations.[16] Also, aluminum induces aggregation of the neurofilament-H and middle molecular neurofilament subunits to form complexes that are relatively resistant to proteolysis. Like other issues, nerve cells contain at least three different pathways for protein breakdown: proteolysis by lysosomal proteases such as cathepsins, proteolysis by non-lysosomal intracellular calcium-dependent proteases such as calpain, and proteolysis by non-lysosomal ATP-ubiquitin-dependent proteolytic proteases that function as multicatalytic protease complexes (proteasomes).[31] These intracellular proteases are thought to participate in the pathogenesis of aluminum-induced neuropathology. Indeed, cathepsin D and calpain activities are increased in the spinal cord and brain after aluminum exposure[26,32] and neurofilament proteins are degraded by these proteases.[33,34] Nixon *et al.*[16] demonstrated that aluminum inhibits calpain-mediated proteolysis of neurofilament proteins, suggesting that inhibition of the process might induce the abnormal accumulation of phosphorylated neurofilament proteins. Despite involvement in the majority of intracellular proteolyses, the role of proteasome has not been examined in aluminum-treated rabbits. A previous report suggested that the proteasome inhibitors lactcystin and N-carboxbenzoxy-leucyl-leucyl-leucinel induce the perikaryal accumulation of phosphorylated neurofilaments and increase apoptosis-specific protein *in vitro*.[35]

Two proteasome forms have been identified: the 26S proteasome, which degrades ubiquitin-conjugated proteins, and the 20S proteasome, which degrades various abnormal proteins in a ubiquitin-independent as well as a ubiquitin-dependent manner.[18,36] Recent studies reported that various proteins, such as tau protein, amyloid precursor protein, and α-synuclein are degraded by the 20S proteasome in a ubiquitin-independent as well as ubiquitin-dependent manner.[21,22,37] These studies suggested that proteasome inhibition might be related to various neurodegenerative disorders. Proteasomes are ubiquitously, but not homogeneously, distributed in the normal rat central nervous system, and are especially abundant in spinal motor neurons and pyramidal cortical neurons.[38] In the present study, immunohistochemistry revealed that the intensity of the 20S proteasome immunoreactivity was significantly increased in the spinal motor neurons from aluminum-treated rabbits as compared with controls. Proteasome activity was also significantly increased in lumbar spinal cord extract from the aluminum-treated rabbits as compared with that in controls. Furthermore, the area and intensity of immunoreaction for 20S proteasome were subsequently decreased with enlargement of SMI 31 positive inclusion, suggesting that 20S proteasome decreases with abnormal aggregation of phosphorylated neurofilament in the cytoplasm of spinal motor neurons. Namely, the immunoreactivity for 20S proteasome was significantly decreased in the cytoplasm of neurons with large phosphorylated neurofilament inclusion than in that with small sized inclusion or without inclusion. Therefore, the massive neurofilament aggregation may be the result of decreased 20S proteasome activity somehow caused through aluminum intoxication. It may be that the decreased immunostaining of 20S proteasome in large inclusion are due to aggregation and insolubility of neurofilament in the cytoplasm of motor neurons.

In vitro study of the degradation of neurofilament-H protein using Western blot first revealed that the 20S proteasome time- and dose-dependently degraded the neurofilament-H proteins, such as calpain and cathepsin. This finding suggests that the 20S proteasome mediates proteolysis of the non-phosphorylated neurofilamentous proteins. It is unclear whether or not 20S proteasome also degrades the phosphorylated neurofilament such as calpain.

In the present study, our immunohistochemistry revealed that neuronal cytoplasmic regions positive for SMI 31 and S20 proteasomes were segregated from each other, even in the neurons with small neurofilamentous inclusions. Small sized SMI 31 positive inclusions were exclusively in the periphery of cytoplasm, and occupied in large parts of cytoplasm with enlargement. This finding suggests that intracellular phosphorylated neurofilaments are formed first in the periphery of cytoplasm in the earlier stage of aluminum intoxication.

Our results suggest that proteasomes may be involved in neurofilament protein turnover and prevent the aggregation of neurofilament proteins. Proteasome activity was significantly increased in lumbar spinal cord extracts from the aluminum-treated rabbits as compared with controls as a whole. The increase of the proteasome activity may indicate a reactive induction of proteasome for aluminum intoxication, or an up-regulation following the aggregation of neurofilament proteins. However, immunoreactivity for 20S proteasome was decreased in the motor neuron with large intracellular phosphorylated neurofilaments as compared with that in small inclusions. Accordingly, the decreased proteasome immunoreactivity may be explained by the loss of protease activity or the over-aggregation and insolubility of neurofilament protein in the enlarged

neurons. The results led us to the following hypothesis: aluminum induces the aggregation of phosphorylated neurofilaments, probably inhibiting dephosphorylation of neurofilaments,[5] despite the lack of inhibition of proteasome activity. And the massive neurofilament might be a result of decreased 20S proteasome activity through aluminum intoxication.

Furthermore, proteasome activation suggests that proteasomes, as well as calpain and cathepsin, might have a role in intracellular proteolysis, especially in the earlier stages of nerve cell degeneration in aluminum-treated rabbits.

ACKNOWLEDGMENTS

We are grateful to Mrs M. Ono, Mrs A. Yasuda, and Mrs K. Hirano for their excellent technical assistance.

REFERENCES

1. Munoz DG, Greene C, Perl DP, Selkoe DJ. Accumulation of phosphorylated neurofilaments in anterior horn motoneurons of amyotrophic lateral sclerosis patients. *J Neuropathol Exp Neurol* 1988; **47**: 9–18.
2. Sobue G, Hashizume Y, Yasuda T *et al.* Phosphorylated high molecular weight neurofilament protein in lower motor neurons in amyotrophic lateral sclerosis and other neurodegenerative diseases involving ventral horn cells. *Acta Neuropathol* 1990; **79**: 402–408.
3. Katsetos CD, Savory J, Herman MM *et al.* Neuronal cytoskeletal lesions induced in the CNS by intraventricular and intravenous aluminium maltol in rabbits. *Neuropathol Appl Neurobiol* 1990; **16**: 511–528.
4. Parhad IM, Krekoski CA, Mathew A, Tran PM. Neuronal gene expression in aluminum myelopathy. *Cell Mol Neurobiol* 1989; **9**: 123–138.
5. Strong MJ, Jakowec DM. 200 kDa and 160 kDa neurofilament protein phosphatase resistance following in vivo aluminum chloride exposure. *Neurotoxicology* 1994; **15**: 799–807.
6. Strong MJ, Mao K, Nerurkar VR, Wakayama I, Yanagihara R, Garruto RM. Dose-dependent selective suppression of light (NFL) and medium (NFM) but not heavy (NFH) molecular weight neurofilament mRNA levels in acute aluminum neurotoxicity. *Mol Cell Neurosci* 1994; **5**: 319–326.
7. Takeda M, Tatebayashi Y, Tanimukai S, Nakamura Y, Tanaka T, Nishimura T. Immunohistochemical study of microtubule-associated protein 2 and ubiquitin in chronically aluminum-intoxicated rabbit brain. *Acta Neuropathol* 1991; **82**: 346–352.
8. Gotow T, Tanaka J, Takeda M. The organization of neurofilaments accumulated in perikaryon following aluminum administration: relationship between structure and phosphorylation of neurofilaments. *Neuroscience* 1995; **64**: 553–569.
9. Klatzo I, Wisniewski H, Streicher E. Experimental production of neurofibrillary degeneration. 1. Light microscopic observation. *J Neuropathol Exp Neurol* 1965; **24**: 187–199.
10. Terry RD, Pena C. Experimental production of neurofibrillary degeneration 2. Electron microscopy, phosphatase histochemistry and electron probe analysis. *J Neuropathol Exp Neurol* 1965; **24**: 200–210.
11. Johnson GV, Jope RS. Phosphorylation of rat brain cytoskeletal proteins is increased after orally administered aluminum. *Brain Res* 1988; **456**: 95–103.
12. Bizzi A, Gambetti P. Phosphorylation of neurofilaments is altered in aluminium intoxication. *Acta Neuropathol* 1986; **71**: 154–158.
13. Strong MJ, Garruto RM. Neuron-specific thresholds of aluminum toxicity in vitro: a comparative analysis of dissociated fetal rabbit hippocampal and motor neuron-enriched cultures. *Lab Invest* 1991; **65**: 243–249.
14. Troncoso JC, Hoffman PN, Griffin JW, Hess-Kozlow KM, Price DL. Aluminum intoxication: a disorder of neurofilament transport in motor neurons. *Brain Res* 1985; **342**: 172–175.
15. Shea TB, Wheeler E, Jung C. Aluminum inhibits neurofilament assembly, cytoskeletal incorporation, and axonal transport. Dynamic nature of aluminium-induced perikaryal neurofilament accumulations as revealed by subunit turnover. *Mol Chem Neuropathol* 1997; **32**: 17–39.
16. Nixon RA, Clarke JF, Logvinenko KB, Tan MK, Hoult M, Grynspan F. Aluminum inhibits calpain-mediated proteolysis and induces human neurofilament proteins to form protease-resistant high molecular weight complexes. *J Neurochem* 1990; **55**: 1950–1959.
17. Shea TB, Balikian P, Beermann ML. Aluminum inhibits neurofilament protein degradation by multiple cytoskeleton-associated proteases. *FEBS Lett* 1992; **307**: 195–198.
18. Coux O, Tanaka K, Goldberg AL. Structure and functions of the 20S and 26S proteasomes. *Annu Rev Biochem* 1996; **65**: 801–847.
19. Tanaka K, Chiba T. The proteasome: a protein-destroying machine. *Genes Cells* 1998; **3**: 499–510.
20. Ding Q, Keller JN. Proteasomes and proteasome inhibition in the central nervous system. *Free Radic Biol Med* 2001; **31**: 574–584.
21. David DC, Layfield R, Serpell L, Narain Y, Goedert M, Spillantini MG. Proteasomal degradation of tau protein. *J Neurochem* 2002; **83**: 176–185.

22. Checler F, da Costa CA, Ancolio K, Chevallier N, Lopez-Perez E, Marambaud P. Role of the proteasome in Alzheimer's disease. *Biochim Biophys Acta* 2000; **1502**: 133–138.
23. Tsuji S, Kikuchi S, Shinpo K *et al.* Proteasome inhibition induces selective motor neuron death in organotypic slice cultures. *J Neurosci Res* 2005; **82**: 443–451.
24. Suzuki H, Takeda M, Nishimura T. Enzymatic characterization of cathepsin D in rabbit brains with experimental neurofibrillary changes. *Biochem Mol Bio Int* 1994; **32**: 1033–1039.
25. Simpson J, Yates CM, Whyler DK, Wilson H, Dewar AJ, Gordon A. Biochemical studies on rabbits with aluminium induced neurofilament accumulations. *Neurochem Res* 1985; **10**: 229–237.
26. Guo-Ross S, Yang E, Bondy SC. Elevation of cerebral proteases after systemic administration of aluminum. *Neurochem Int* 1998; **33**: 277–282.
27. Yamamoto T, Hirano A. A comparative study of modified Bielschowsky Bodian and thioflavin S stains on Alzheimer's neurofibrillary tangles. *Neuropathol Appl Neurobiol* 1986; **12**: 3–9.
28. Lowry OH, Rosenbrough NJ, Farr L, Randall RJ. Protein measurement with the Folin phenol reagent. *J Biol Chem* 1951; **193**: 265–275.
29. Laemmli UK. Cleavage of structural proteins during the assembly of the head of bacteriophage T4. *Nature* 1970; **227**: 680–685.
30. Strong MJ, Strong WL, Jaffe H, Traggert B, Sopper MM, Pant HC. Phosphorylation state of the native high-molecular-weight neurofilament subunit protein from cervical spinal cord in sporadic amyotrophic lateral sclerosis. *J Neurochem* 2001; **76**: 1315–1325.
31. Mitch WE, Goldberg AL. Mechanisms of muscle wasting. The role of the ubiquitin-proteasome pathway. *N Engl J Med* 1996; **335**: 1897–1905.
32. Suzuki H, Takeda M, Nakamura Y, Tada K, Hariguchi S, Nishimura T. Activities of lysosomal enzymes in rabbit brain with experimental neurofibrillary changes. *Neurosci Lett* 1988; **89**: 234–239.
33. Banay-Schwartz M, Dahl D, Hui KS, Lajtha A. The breakdown of the individual neurofilament proteins by cathepsin D. *Neurochem Res* 1987; **12**: 361–367.
34. Malik MN, Sheikh AM, Fenko MD, Wisniewski HM. Purification an degradation of purified neurofilament proteins by the brain calcium-activated neutral proteases. *Life Sci* 1986; **39**: 1335–1343.
35. Masaki R, Saito T, Yamada K, Ohtani-Kaneko R. Accumulation of phosphorylated neurofilaments and increase in apoptosis-specific protein and phosphorylated c-Jun induced by proteasome inhibitors. *J Neurosci Res* 2000; **62**: 75–83.
36. Benaroudj N, Tarcsa E, Cascio P, Goldberg AL. The unfolding of substrates and ubiquitin-independent protein degradation by proteasomes. *Biochimie* 2001; **83**: 311–318.
37. Tofaris GK, Layfield R, Spillantini MG. Alpha-synuclein metabolism and aggregation is linked to ubiquitin-independent degradation by the proteasome. *FEBS Lett* 2001; **509**: 22–26.
38. Mengual E, Arizti P, Rodrigo J, Gimenez-Amaya JM, Castano JG. Immunohistochemical distribution and electron microscopic subcellular localization of the proteasome in the rat CNS. *J Neurosci* 1996; **16**: 6331–6341.

Original Paper

International Archives of Allergy and Immunology

Int Arch Allergy Immunol 2007;142:285–290
DOI: 10.1159/000097359

Received: May 2, 2006
Accepted after revision: July 27, 2006
Published online: November 22, 2006

Elevated Soluble ADAM8 in Bronchoalveolar Lavage Fluid in Patients with Eosinophilic Pneumonia

Osamu Matsuno[a] Eishi Miyazaki[a] Shinichi Nureki[a] Takuya Ueno[a]
Masaru Ando[a] Kazunobu Ito[b] Toshihide Kumamoto[a] Yasunori Higuchi[c]

[a]Division of Respiratory Disease, Department of Brain and Nerve Science and [b]Research Center for Applied Medical Engineering, Oita University Faculty of Medicine, Yufu City, and [c]Shin-Beppu Hospital, Beppu City, Japan

Key Words
ADAM8 · VCAM-1 · CD23 · Eosinophilic pneumonia

Abstract
Background: ADAM (a disintegrin and metalloprotease) family members, characterized by a metalloprotease and a disintegrin domain, are membrane-anchored glycoproteins involved in proteolysis and cell adhesion. ADAM8 might have an important role in allergic inflammation. It can cleave a variety of substrates and is a sheddase for VCAM-1 and CD23, the low-affinity IgE receptors. ***Methods:*** To evaluate the contribution of ADAM8 to the pathogenesis of eosinophilic pneumonia (EP), we measured the concentrations of soluble ADAM8 (sADAM8) and its substrates, soluble VCAM-1 (sVCAM-1) and soluble CD23 (sCD23), in bronchoalveolar lavage fluid from patients with smoking-induced acute eosinophilic pneumonia (AEP), chronic idiopathic eosinophilic pneumonia (CEP), and drug-induced eosinophilic pneumonia (drug-EP). ***Results:*** The sADAM8 and sVCAM-1 concentrations were increased in AEP and CEP. The sCD23 concentration was elevated in AEP. In AEP, but not CEP, the sADAM8 concentration significantly correlated with those of both sVCAM and sCD23. ***Conclusion:*** The pathogenesis of AEP, CEP, and drug-EP was distinct with regard to ADAM8. Our results are the first to associate ADAM8 with eosinophilic responses and lung inflammation in humans.

Introduction

Eosinophilic pneumonia (EP) is defined as pulmonary infiltration of eosinophils independent of peripheral blood eosinophilia. This pulmonary disorder includes clinically different types of EP, such as acute idiopathic eosinophilic pneumonia (AEP), chronic idiopathic eosinophilic pneumonia (CEP), and drug-induced eosinophilic pneumonia (drug-EP). Although there are a few reports comparing the clinical characteristics of these different forms of EP [1–4], there are no reports that describe the pathogenesis of these different forms.

ADAM family members are implicated to be involved in the proteolytic processing of membrane-bound precursors, and they modulate cell-cell and cell-matrix interactions. ADAM8 has metalloprotease activity in vitro and catalyzes VCAM-1 and CD23, the low-affinity IgE receptor [5, 6]. VCAM-1, a member of the immunoglobulin supergene family of adhesion molecules, is important for eosinophil recruitment in allergic disorders [7, 8]. CD23 has an important role in the modulation of allergic pulmonary inflammation, likely mediated by negative signaling [9, 10]. To our knowledge, there are no reports that describe the roles of VCAM-1 or CD23 in EP, although both molecules have an important role in allergic inflammation.

ADAM8 (also called CD156a) is specifically induced in experimental asthma and is highly expressed in hu-

KARGER
Fax +41 61 306 12 34
E-Mail karger@karger.ch
www.karger.com

1018–2438/07/1424–0285$23.50/0

Accessible online at:
www.karger.com/iaa

Correspondence to: Dr. Osamu Matsuno
Division of Respiratory Disease, Department of Brain and Nerve Science
Oita University Faculty of Medicine, Idaigaoka 1-1
Hazama-machi, Yufu City, Oita 879-5593 (Japan)
Tel. +81 97 586 5814, Fax +81 97 586 6502, E-Mail matsuno@med.oita-u.ac.jp

Table 1. Patient details

Case	Sex (male/female)	Age years	Total cells $\times 10^5$ cells/ml	Eosinophils %	Lymphocytes %	Macrophages %	CD4/8
AEP (n = 10)	8/2	18.7 ± 0.73	6.73 ± 1.23	55.40 ± 5.99	18.51 ± 3.66	19.09 ± 3.33	2.23 ± 0.45
CEP (n = 10)	3/7	60.4 ± 5.68	9.48 ± 2.85	50.98 ± 8.09	10.77 ± 5.44	33.57 ± 6.70	2.05 ± 0.14
Drug-EP (n = 7)	3/4	64.0 ± 7.30	5.74 ± 2.46	31.37 ± 2.65	19.53 ± 4.92	37.60 ± 7.77	1.11 ± 0.35
IPF (n = 10)	7/3	61.5 ± 2.11	3.21 ± 0.41	2.83 ± 1.11	13.96 ± 6.33	76.23 ± 6.92	2.72 ± 0.68
Sar (n = 10)	4/6	55.2 ± 2.90	2.82 ± 0.48	1.81 ± 1.74	20.16 ± 7.72	77.10 ± 9.07	6.99 ± 1.89
HV (n = 10)	8/2	26.6 ± 0.97	1.58 ± 0.30	0.7 ± 0.45	3.95 ± 0.92	94.16 ± 1.41	2.05 ± 0.45

Data are expressed as mean ± SEM.

man eosinophils [10, 11]. We previously reported that soluble ADAM8 (sADAM8) significantly inhibits experimental asthma [12]. In the present study, we extend our earlier study by measuring sADAM8, soluble VCAM-1 (sVCAM-1), and soluble CD23 (sCD23) in bronchoalveolar lavage fluid (BALF) in EP. The findings reported in the present study are the first to demonstrate that sADAM8 is increased in eosinophilic inflammation in humans.

Methods

Patients

Patients' backgrounds are summarized in table 1. The 26 patients with EP (10 patients with smoking-induced AEP, 10 patients with CEP, and 6 patients with drug-EP) were diagnosed at the Oita University Faculty of Medicine Hospital and related hospitals from 1999 to 2004. Pulmonary eosinophilia was detected by bronchoalveolar lavage (BAL) and transbronchial lung biopsy specimens. AEP was diagnosed according to the criteria described by Allen et al. [13]. Most patients with AEP showed spontaneous improvement, although 2 patients required corticosteroid therapy for a few days. The diagnosis of CEP was made based on the diagnostic criteria of CEP described by Carrington et al. [14]. All patients were treated with corticosteroids. The patients with drug-EP satisfied the following diagnostic criteria: fever or some respiratory symptoms, diffuse pulmonary infiltrates on chest X-ray films, increased percentage of eosinophils in BALF, prompt improvement after cessation of the causative drug, absence of other possible causes, positive reaction in lymphocyte stimulation assays, or recurrence of the symptoms with drug challenge. We also studied a control group of 30 patients with noneosinophilic lung disease: 10 patients with idiopathic pulmonary fibrosis (IPF), 10 patients with sarcoidosis (Sar) and 10 healthy volunteers (HV). The patients with usual interstitial pneumonia associated with collagen vascular diseases were excluded in this study. In all 10 IPF cases, the diagnosis was pathologically confirmed as usual interstitial pneumonia. Sar was diagnosed on the basis of typical clinical features and the presence of epithelioid cell granulomas in biopsy specimens from the lung, skin, or lymph nodes. All tests were performed in the context of routine medical care of the patients. None of the patients was treated with glucocorticoids before BAL procedures were completed. Written informed consent was provided by the HV.

Bronchoalveolar Lavage

BAL was performed as described previously [15] in an affected lung segment using three 50-ml aliquots of saline solution. The differential cell count was determined by cytocentrifugation followed by Wright staining. Fluid samples were processed immediately for cytological and microbiological analysis. No organism was cultured from the BAL culture. Cytology was negative for malignant cells.

Determination of sADAM8, sVCAM-1 and sCD23 in BALF

sADAM8, sVCAM-1 and sCD23 concentrations in BALF were measured using a commercially available enzyme-linked immunosorbent assay (ELISA) kit according to the manufacturer's protocol. A Quantikine kit from R&D Systems (Minneapolis, Minn., USA) was used to quantify sADAM8. An immunoassay kit from Biosource (Camarillo, Calif., USA) was used to quantify sVCAM-1. A human sCD23 ELISA kit (Bender MedSystems, Vienna, Austria) was used to quantify CD23. The minimal detectable levels were 5.27 pg/ml (sADAM8), 0.5 ng/ml (sVCAM-1), and 6.8 U/ml (sCD23).

Statistics

The Kruskall-Wallis test was used to compare values between groups. In case of a significant difference between groups, data were analyzed by the Mann-Whitney U test. Correlation coefficients were determined by Pearson's linear regression analysis between sADAM8, sVCAM-1 and sCD23. Correlation coefficients between serial changes in ADAM8 concentration and the delay in obtaining BAL after the clinical onset were determined by Spearman's method. A difference was considered significant when the p value was less than 0.05.

Results

sADAM8, sVCAM-1 and sCD23 Concentration in BALF from Various Diffuse Lung Diseases

sADAM8, sVCAM-1 and sCD23 concentrations were measured by ELISA. They were not significantly elevated

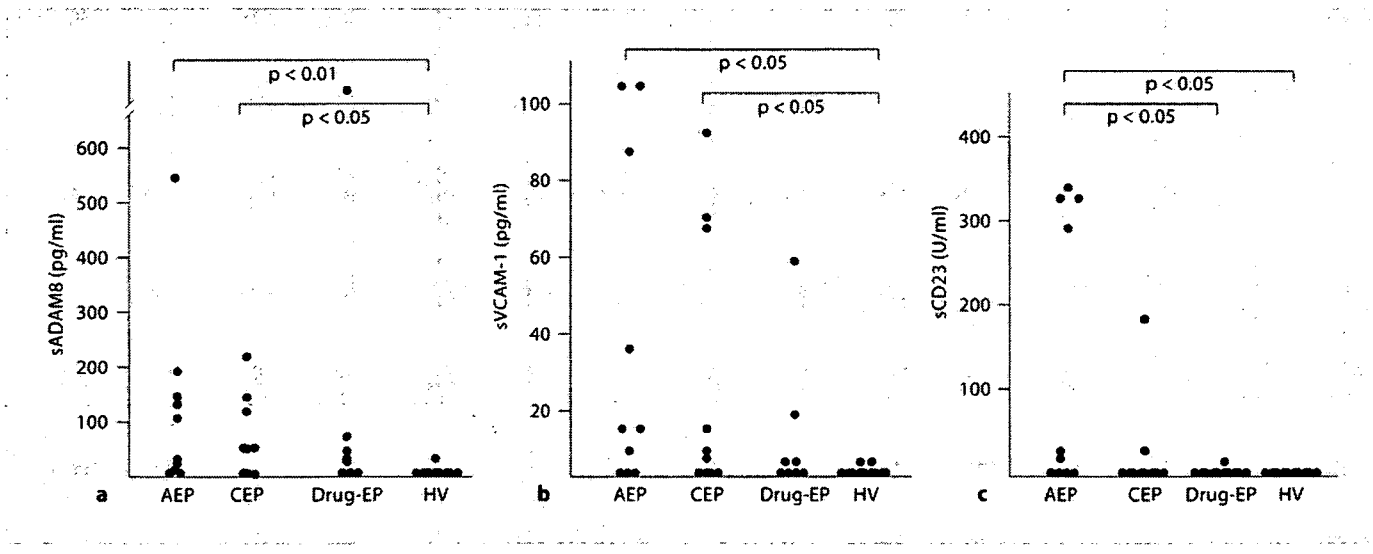

Fig. 1. Concentration of ADAM8 (**a**), VCAM-1 (**b**) and CD23 (**c**) in BALF obtained from patients with smoking-induced AEP, CEP, drug-EP and HV. Significant differences are shown at the top.

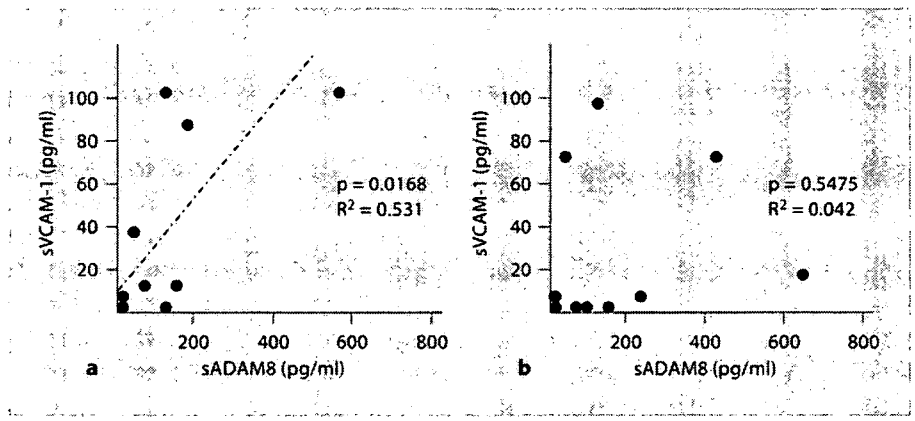

Fig. 2. Relationship between ADAM8 and VCAM-1 concentrations in BALF from patients with AEP ($R^2 = 0.531$) (**a**) and CEP (**b**).

in noneosinophilic conditions, such as IPF and Sar (data not shown). The sADAM8 concentrations were significantly elevated in AEP ($p < 0.01$) and CEP ($p < 0.05$), when compared to HV (fig. 1a). There was no significant difference in BALF ADAM8 concentrations between different types of EP (fig. 1a). The sVCAM-1 concentrations were significantly elevated in AEP ($p < 0.05$) and CEP ($p < 0.05$), when compared to HV (fig. 1b). There was no significant difference in BALF VCAM-1 concentrations between different types of EP (fig. 1b). The CD23 concentrations were significantly elevated in AEP alone ($p < 0.05$; fig. 1c). sCD23 in the BALF were significantly elevated in AEP when compared to IPF, Sar and HV ($p < 0.05$) (data not shown). In addition, there was a significant difference in BALF CD23 concentration between AEP and drug-EP ($p < 0.05$; fig. 1c). BALF sADAM8, sVCAM-1 and sCD23 concentrations were not significantly elevated in drug-EP.

Relationship between sADAM8, sVCAM-1 and sCD23 in BALF

There was significant correlation between sADAM8 and sVCAM-1 concentrations in the BALF from AEP ($p < 0.05$; fig. 2a), but not from CEP (fig. 2b), although sADAM8 and sVCAM-1 concentrations were significantly elevated in both AEP and CEP. There was also a

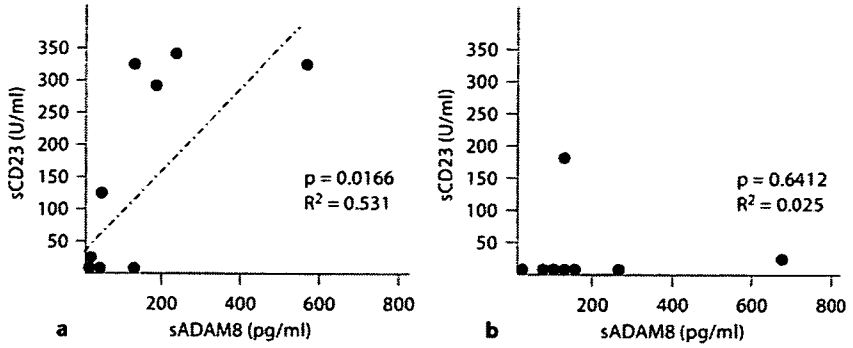

Fig. 3. Relationship between ADAM8 and CD23 concentration in BALF from patients with AEP (p = 0.0166) (**a**) and CEP (p = 0.6412) (**b**).

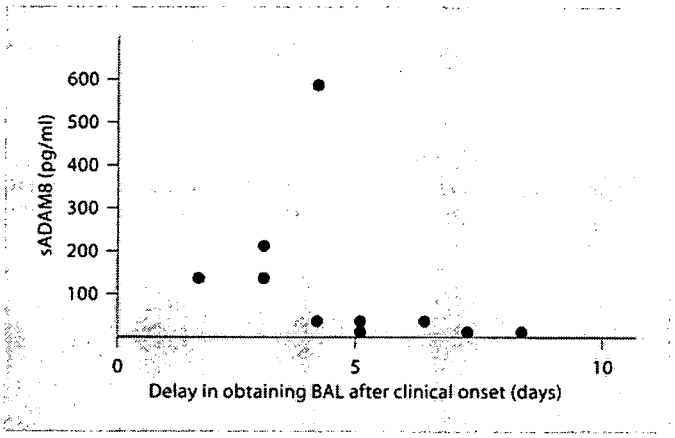

Fig. 4. Serial changes in ADAM8 concentration and the delay in obtaining BAL after clinical onset of AEP ($p < 0.05$).

significant correlation between the BALF sADAM8 and sCD23 concentrations from AEP ($p < 0.05$; fig. 3a), but not from CEP (fig. 3b). These results suggest that ADAM8 was the main sheddase for VCAM-1 in AEP, but not CEP. In addition, CD23 was associated with AEP alone, but not CEP or drug-EP.

Serial Changes in ADAM8 Concentration and the Delay in Obtaining BAL after Clinical Onset

There was a negative correlation between BALF ADAM8 concentrations and the delay in obtaining BAL after the clinical onset of AEP (fig. 4). Prednisone treatment could not be responsible for the decline in ADAM8, because all BAL were performed before treatment.

Discussion

ADAM family proteins are associated with asthma. A recent human genome search revealed that polymorphism or mutation of the ADAM33 gene was associated with bronchial hyperresponsiveness [16]. The potential importance of ADAM8 in eosinophil inflammation is also highlighted by a reported microarray analysis of whole lung from mice in which ADAM8 was one of the mRNAs upregulated after antigen challenge with ovalbumin [11]. Eosinophils are a major source of ADAM8 mRNA [8]. Gene-targeted mouse studies revealed that ovalbumin-induced ADAM8 is largely dependent on signal transduction and activation of STAT-6 and IL-4 α-chain [11]. Although ADAM8 had not been studied in the context of allergy or lung inflammation in humans, a recent study identified CD23 and VCAM-1 as specific substrates for the metalloproteinase associated with ADAM8 [5, 6]. We previously presented the first evidence that sADAM8 has a physiologic role in protecting against allergic pulmonary disease in experimental murine asthma [12]. The ADAM8 concentrations were significantly elevated in AEP and CEP when compared to HV. These results indicate that ADAM8 is associated with allergic lung inflammation in humans.

Eosinophils degrade VCAM-1 in a metalloprotease-dependent manner. VCAM-1 is expressed on the surface of cultured endothelial cells in response to mediators of Th2 immunity and in blood vessels of biopsies from patients with asthma [17, 18]. VCAM-1 supports α_4 integrin-mediated tethering, rolling, and migration of lymphocytes and rolling of eosinophils [19]. Degradation of VCAM-1 might be necessary for eosinophil transmigration through activated endothelium and subendothelial basement membrane. Activated endothelium might re-

lease soluble forms of VCAM-1 that can be detected in the blood and BALF [20]. sVCAM-1 concentrations in the BALF were significantly elevated in the EP group. The sVCAM-1 concentrations were significantly elevated in AEP and CEP, when compared to HV. The findings of the present study are, to our knowledge, the first to demonstrate the elevated levels of sVCAM-1 in EP. There was a significant correlation between the ADAM8 and VCAM-1 concentrations in BALF from AEP, but not from CEP. These results might indicate that degradation of VCAM-1 in AEP is regulated by ADAM8; on the other hand, degradation of VCAM-1 in CEP is regulated by a protease other than ADAM8, such as ADAM17 or other proteases [21].

ADAM8 is able to convert membrane-bound CD23 into a soluble form that might be involved in the regulation of IgE synthesis and activation of macrophages to release a variety of proinflammatory mediators, although the role of sCD23 is not well-known in human allergic lung inflammation. Mice deficient in CD23 produce higher levels of IgE than their wild-type counterparts [22] without any effect on B cell or T cell growth and differentiation [22–24]. Conversely, mice overexpressing membrane CD23 exhibit a weaker IgE response [25]. In contrast, CD23 knockout mice are unable to demonstrate an antigen-specific IgE-mediated antibody response [23]. CD23 negatively regulates pulmonary inflammation and acute bronchial hyperresponsiveness [9, 10]. The CD23 concentrations were significantly elevated in AEP compared to drug-EP, IPF, Sar and HV. The findings reported in the present study are the first to demonstrate the elevation of CD23 in EP, especially AEP. These results indicate that CD23 might have an important role in the pathogenesis of AEP, but not CEP and drug-EP. In addition, there was also a significant correlation between the sADAM8 and sCD23 concentrates in BALF from AEP. These results also suggest that ectodomain shedding of CD23 in AEP is regulated by ADAM8.

sADAM8, sVCAM-1 and sCD23 concentrations in the BALF were not elevated in drug-EP, indicating the possibility that drug-EP is a different disease condition. ADAM8 might not be associated with the pathogenesis of drug-EP, although ADAM8 in BALF is significantly elevated in AEP and CEP.

Serial changes in sADAM8 concentration and the delay in obtaining BAL after clinical onset demonstrated a negative correlation between sADAM8 in BALF and the delay in obtaining BAL after clinical onset in AEP. These results indicate that ADAM8 acts primarily at the earlier stage of eosinophilic inflammation of AEP. King et al. [11] also reported that ADAM8 induction initially parallels the cellular infiltrate into the BALF after allergen challenge, whereas ADAM8 induction and cellular infiltrate are dissociated by late phase [6].

It is expected that another ADAM8 mechanism might be involved in allergic lung inflammation. The disintegrin domain of ADAM8 affects cell adhesion [26, 27]. The ADAM8 disintegrin domain might involve neural cell adhesion and has a protective effect on experimental encephalomyelitis [27]. Presently, however, the role of the disintegrin domain of ADAM8 in the allergy or lung inflammation is not known. Further examination is necessary to evaluate it.

The difference in the ADAM8 concentrations as well as its relation to VCAM-1 and CD23 concentrations indicate that the pathogenesis of AEP, CEP and drug-EP is distinct, although the accumulation of eosinophils in the lungs is a common feature. Our results contribute to improving the recognition of AEP, CEP and drug-EP, and warrant further evaluation, which will lead to a better understanding of the full spectrum of EP. Additional studies to identify the unknown substrates of ADAM8 in allergic lung inflammation might contribute not only to the identification of novel markers and therapeutic targets, but should also yield new understanding of the signaling pathway mediated by ADAM8 expression.

References

1 Hayakawa H, Sato A, Toyoshima M, et al: A clinical study of idiopathic eosinophilic pneumonia. Chest 1994;105:1462–1466.
2 Fujimura M, Yasui M, Shinagawa S, et al: Bronchoalveolar lavage cell findings in three types of eosinophilic pneumonia: acute, chronic and drug-induced eosinophilic pneumonia. Respir Med 1998;92:743–749.
3 Nakahara Y, Hayashi S, Fukuno Y, et al: Increased interleukin-5 levels in bronchoalveolar lavage fluid is a major factor for eosinophil accumulation in acute eosinophilic pneumonia. Respiration 2001;68:389–395.
4 Mochimaru H, Kawamoto M, Fukuda Y, et al: Clinicopathological differences between acute and chronic eosinophilic pneumonia. Respirology 2005;10:76–85.
5 Johansson MW, Lye MH, Barthel SR, et al: Eosinophils adhere to vascular cell adhesion molecule-1 via podosomes. Am J Respir Cell Mol Biol 2004;31:413–422.
6 Fourie AM, Coles F, Moreno V, et al: Catalytic activity of ADAM8, ADAM15, and MDC-L (ADAM28) on synthetic peptide substrates and in ectodomain cleavage of CD23. J Biol Chem 2003;278:30469–30477.

7 Hakansson L, Bjornsson E, Janson C, et al: Increased adhesion to vascular cell adhesion molecule-1 and intercellular adhesion molecule-1 of eosinophils from patients with asthma. J Allergy Clin Immunol 1995;96: 941–950.
8 Chin JE, Hatfield CA, Winterrowd GE, et al: Airway recruitment of leukocytes in mice is dependent on alpha4-integrins and vascular cell adhesion molecule-1. Am J Physiol 1997; 272:L219–L229.
9 Cernadas M, De Sanctis GT, Krinzman SJ, et al: CD23 and allergic pulmonary inflammation: potential role as an inhibitor. Am J Respir Cell Mol Biol 1999;20:1–8.
10 Riffo-Vasquez Y, Spina D, Thomas M, et al: The role of CD23 on allergen-induced IgE levels, pulmonary eosinophilia and bronchial hyperresponsiveness in mice. Clin Exp Allergy 2000;30:728–738.
11 King NE, Zimmermann N, Pope SM, et al: Expression and regulation of a disintegrin and metalloproteinase (ADAM) 8 in experimental asthma. Am J Respir Cell Mol Biol 2004;31:257–265.
12 Matsuno O, Miyazaki E, Nureki S, et al: Role of ADAM8 in experimental asthma. Immunol Lett 2006;102:67–73.
13 Allen JN, Pacht ER, Gadek JE, et al: Acute eosinophilic pneumonia as a reversible cause of noninfectious respiratory failure. N Engl J Med 1989;321:569–574.
14 Carrington CB, Addington WW, Goff AM, et al: Chronic eosinophilic pneumonia. N Engl J Med 1969;280:787–798.
15 Crystal RG, Bitterman PB, Rennard SI, et al: Interstitial lung diseases of unknown cause. Disorders characterized by chronic inflammation of the lower respiratory tract. N Engl J Med 1984;310:154–166.
16 Van Eerdewegh P, Little RD, Dupuis J, et al: Association of the ADAM33 gene with asthma and bronchial hyperresponsiveness. Nature 2002;418:426–430.
17 Lee YW, Kuhn H, Hennig B, et al: IL-4-induced oxidative stress upregulates VCAM-1 gene expression in human endothelial cells. J Mol Cell Cardiol 2001;33:83–94.
18 Gosset P, Tillie-Leblond I, Janin A, et al: Expression of E-selectin, ICAM-1 and VCAM-1 on bronchial biopsies from allergic and nonallergic asthmatic patients. Int Arch Allergy Immunol 1995;106:69–77.
19 Rose DM, Han J, Ginsberg MH: Alpha4 integrins and the immune response. Immunol Rev 2002;186:118–124.
20 Zangrilli JG, Shaver JR, Cirelli RA, et al: sVCAM-1 levels after segmental antigen challenge correlate with eosinophil influx, IL-4 and IL-5 production, and the late phase response. Am J Respir Crit Care Med 1995;151: 1346–1353.
21 Garton KJ, Gough PJ, Philalay J, et al: Stimulated shedding of vascular cell adhesion molecule 1 (VCAM-1) is mediated by tumor necrosis factor-alpha-converting enzyme (ADAM 17). J Biol Chem 2003;278:37459–37464.
22 Yu P, Kosco-Vilbois M, Richards M, et al: Negative feedback regulation of IgE synthesis by murine CD23. Nature 1994;369:753–756.
23 Fujiwara H, Kikutani H, Suematsu S, et al: The absence of IgE antibody-mediated augmentation of immune responses in CD23-deficient mice. Proc Natl Acad Sci USA 1994; 91:6835–6839.
24 Stief A, Texido G, Sansig G, et al: Links mice deficient in CD23 reveal its modulatory role in IgE production but no role in T and B cell development. J Immunol 1994;152:3378–3390.
25 Texido G, Eibel H, Le Gros G, et al: Transgene CD23 expression on lymphoid cells modulates IgE and IgG1 responses. J Immunol 1994;153:3028–3042.
26 Schlomann U, Wildeboer D, Webster A, et al: The metalloprotease disintegrin ADAM8. Processing by autocatalysis is required for proteolytic activity and cell adhesion. J Biol Chem 2002;277:48210–48219.
27 Schluesener HJ: The disintegrin domain of ADAM 8 enhances protection against rat experimental autoimmune encephalomyelitis, neuritis and uveitis by a polyvalent autoantigen vaccine. J Neuroimmunol 1998;87:197–202.

Letter to the Editor

European Neurology

Eur Neurol 2007;57:111–113
DOI: 10.1159/000098063

Received: April 21, 2006
Accepted: September 22, 2006
Published online: December 15, 2006

Encephalitis of Unknown Etiology with Anti-GluR ε2 Autoantibody, Showing Divergent Neuroradiologic and Clinical Findings

Masaki Miyazaki[a] Aihide Yoshino[a] Toshiya Teraishi[a] Soichiro Nomura[a]
Hideaki Nemoto[b] Yukitoshi Takahashi[c]

[a]Department of Psychiatry, National Defense Medical College, Saitama, [b]Department of Neurology, Kohnodai Hospital, National Center of Neurology and Psychiatry, Chiba, and [c]Department of Pediatrics, National Epilepsy Center, Shizuoka Institute of Epilepsy and Neurological Disorders, Shizuoka, Japan

Dear Sir,

A patient with severe temporal lobe atrophy, memory disturbance, and personality deterioration caused by encephalitis of unknown etiology was admitted for evaluation. Cerebrospinal fluid (CSF) studies disclosed no virus, but autoantibodies were detected against the N-methyl-D-aspartate-type glutamate receptor epsilon 2 (GluR ε2). GluR ε2 channels have been implicated in synaptic plasticity and localization associated with neural development and learning [1]. Recently autoantibodies against GluR ε2 were found in some patients with Rasmussen's encephalitis [2] and nonherpetic limbic encephalitis [3], suggesting an autoimmune pathogenesis for some encephalitis. Surprisingly in our case, neuropsychiatric symptoms did not worsen when progressively severe neuroradiologic alterations in the temporal lobes appeared after hospitalization.

Case Report

A 36-year-old man was admitted to our hospital for evaluation concerning the etiology of severe memory impairment. Neither he nor family members had a prior history of epilepsy, dementia, autoimmune diseases, or neuropsychiatric disorders. He had no previous history of alcohol and/or drug abuse. He had been diagnosed with diabetes 2 years previously, but was lost to follow-up before any treatment. He had had a headache which lasted for several days 5 months before admission to our hospital. A short time later he developed severe memory impairment and pathologically increased appetite; he repeatedly stole food, even eating pet foods.

Table 1 presents laboratory, neuropsychologic, electroencephalographic, and neuroradiologic findings over time. Biochemical examinations were normal except for a serum glucose concentration of 320 mg/dl and a glycosylated hemoglobin (HbA1c) value of 15.7%. Antibodies in the serum for HIV and syphilis were negative. The Wechsler Adult Intelligence Scale-Revised (WAIS-R) showed a verbal intelligence quotient (VIQ) of 85, a performance IQ (PIQ) of 85, and a full scale IQ (FIQ) of 84. The Wechsler Memory Scale-Revised (WMS-R) showed very poor general memory, visual memory, verbal memory, and delayed-recall memory (scores of <50, 64, <50, and <50, respectively), while the score on the attention-concentration scale was within the normal range (a score of 106). Electroencephalography (EEG) showed normal background activity and no epileptic discharges. Routine CSF study showed no abnormalities except for moderate elevation of protein (60 mg/dl; normal range 10–40). CSF cell count was 3/mm^3 (normal range 1–6).

MRI of the brain demonstrated severe diffuse cerebral atrophy, with accentuation in the mesial temporal lobes including the hippocampi (fig. 1A), which was suggestive of progressive dementia. However, repeat MRI (fig. 1B) on the 13th hospital day disclosed a new area of high signal intensity centered at the right superior temporal gyrus, suggesting progressive encephalitis. Despite this striking signal alteration, CSF protein and cell counts were within the normal range on three occasions, days 14, 49, and 88. Body temperature remained within the normal range throughout the course of illness. Polymerase chain reaction (PCR) did not detect herpes simplex virus (HSV)-1 or 2, human herpes virus-6 or 7, cytomegalovirus, or Epstein-Barr virus in the CSF on days 49 or 88. Systemic radiologic examination did not disclose a malignant neoplasm while anti-Hu antibodies were not detected in the CSF at a dilution of 1:2,000 by Western blotting, probably excluding paraneoplastic limbic encephalitis. Blood sugar remained well below 200 mg/dl.

KARGER

Fax +41 61 306 12 34
E-Mail karger@karger.ch
www.karger.com

0014–3022/07/0572–0111$23.50/0

Accessible online at:
www.karger.com/ene

Aihide Yoshino, MD
Department of Psychiatry, National Defense Medical College
3–2 Namiki, Tokorozawa
Saitama 3598513 (Japan)
Tel. +81 4 2995 1619, Fax +81 4 2996 5203, E-Mail aihide@ndmc.ac.jp

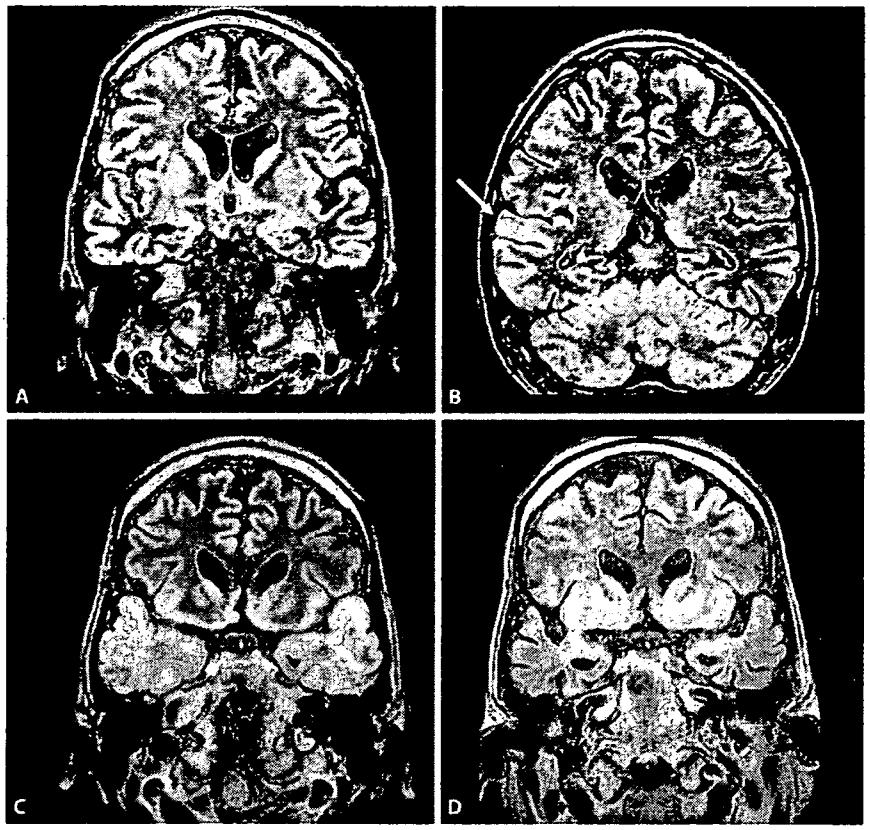

Fig. 1. Coronal FLAIR MRI sequences. **A** Day 4: diffuse cerebral atrophy is seen, especially in the mesial temporal lobes including the hippocampi. **B** Day 13: a new area of high signal intensity is centered in the right superior temporal gyrus. **C** Day 46: severe signal alteration with edema affects extensive areas of the temporal lobes. **D** Day 172: abnormal signal disappeared and brain atrophy remained the same as on day 4 (**A**).

Table 1. Laboratory, clinical, and neuroradiologic course

	Hospital day																		
	0	10	20	30	40	50	60	70	80	90	100	110	120	130	140	150	//	300
CSF																		
Cell count	3		1			0				2								
Protein	60		37			34				40								
Anti-Hu			negative															
Anti-GluR										positive								
Viral DNA PCR						negative				negative								
WAIS-R (FIQ)	84								91							116		90
WMS-R																		
General	<50								59		58					61		<50
Attention	106								101		113					113		101
EEG BGA	8-IIz alpha				9 IIz alpha					9-IIz alpha								9-IIz alpha
MRI	↑ general atrophy		↑ right temporal high intensity		↑ bil. temporal high intensity			↑ bil. temporal high intensity							↑ high intensity: disappeared	↑ general atrophy only		

BGA = Background activity; bil. = bilateral.

On day 46, MRI showed that the severe signal alteration with edema had extended to wide areas of the temporal lobes (fig. 1C). Diffusion-weighted image (DWI) also demonstrated new areas of high intensity at the temporal lobes. Moreover, ^{99m}Tc single-photon emission computed tomography (SPECT) showed significant hyperperfusion in mesial and lateral portions of both temporal lobes, suggesting encephalitis of unknown etiology localized to the temporal lobes. Surprisingly, however, the neuropsychiatric status did not deteriorate, and disturbances of consciousness or epileptic seizures did not occur. On reexamination, WAIS-R and WMS-R showed no significant change (VIQ 85, PIQ 100, FIQ 84, and a score of 101 on the attention-concentration scale). MRI findings had not improved by day 74 despite 10 days of acyclovir therapy. CSF immunoassay for 14-3-3 protein was negative, suggesting that broad, persistent neural injury was not actively progressing. Repeated EEG showed no abnormalities of background activity or epileptic discharges. The patient did not manifest any epileptic seizures, including epilepsia partialis continua and nonconvulsive status epilepticus. Although we did not examine CSF for myelin basic protein or oligoclonal bands, acute disseminated encephalomyelitis was unlikely since MRI signal alterations were diffuse rather than scattered, and repeated EEGs were within the normal ranges.

CSF obtained on day 88 was then examined for autoantibodies against GluR ε2, as these have been reported in some patients with nonherpetic limbic encephalitis [3]. Serum and CSF were tested for anti-GluR ε2 at dilutions of 1:20 and 1:15, respectively. Only CSF IgG, not IgM, autoantibodies were demonstrated. On day 172, the extent of signal alteration clearly had decreased, and the abnormal signal subsequently disappeared (fig. 1D). Overall brain atrophy remained the same as on admission. SPECT showed the disappearance of hyperperfusion in the temporal lobes; the mesial temporal areas now showed hypoperfusion. A third WAIS-R and WMS-R examination showed no notable change. Symptoms and neuroradiologic findings have remained stable after discharge from the hospital.

Discussion

We suspected that the patient initially might have had encephalitis of unknown etiology with severe residual memory impairment and marked atrophy of the mesial temporal cortex. We have had no similar clinical experience in which the first insult causing severe memory impairment was not evident as a history of disturbance of consciousness or epileptic seizure. Five months after the presumed first insult, findings indicated an encephalitis of uncertain etiology showing a marked discrepancy between worsening MRI findings and stable clinical status. Although MRI and SPECT showed severe signal alteration with hyperperfusion in the temporal lobes, neuropsychiatric symptoms did not deteriorate. We know of no reported case of encephalitis with such a divergent clinicoradiologic course. A previously reported case of nonherpetic limbic encephalitis in which neuroradiologic findings disappeared after 6 months showed no relapse [4]. Since some relapsing cases of herpetic encephalitis did not have HSV detectable in CSF by PCR [5], we could not exclude the possibility that his first insult represented herpetic encephalitis, but few clinical symptoms characteristic of herpetic encephalitis were present.

Although the patient's illness may have been caused by an undetected infectious agent, we would propose a different explanation: autoimmune encephalitis. A cell-mediated immune response may have caused tissue damage during an infectious episode 5 months before admission, resulting in production of autoantibodies against GluR ε2. Alternatively, antibodies developing in response to the infectious agent may later have acted as autoantibodies against GluR ε2 because of molecular homology.

Apparent clinical stability in the presence of dramatically worsening neuroradiologic findings during hospitalization may have reflected an initial insult before admission so severe that the WAIS-R and WMS-R could not detect a further decline in temporal lobe function during the admission. Although we could not determine whether autoantibodies against GluR ε2 were the cause or the result of the encephalitis of unknown etiology, we believe that the autoantibodies had a profound influence on the neuroradiologic course.

References

1 Mori H, Manabe T, Watanabe M, Satoh Y, Suzuki N, Toki S, Nakamura K, Yagi T, Kushiya E, Takahashi T, Inoue Y, Sakimura K, Mishina M: Role of the carboxy-terminal region of the GluR epsilon2 subunit in synaptic localization of the NMDA receptor channel. Neuron 1998;21:571–580.

2 Takahashi Y, Mori H, Mishina M, Watanabe M, Fujiwara T, Shimomura J, Aiba H, Miyajima T, Saito Y, Nezu A, Nishida H, Imai K, Sakaguchi N, Kondo N: Autoantibodies to NMDA receptor in patients with chronic forms of epilepsia partialis continua. Neurology 2003;61:891–896.

3 Mochizuki Y, Mizutani T, Isozaki E, Ohtake T, Takahashi Y: Acute limbic encephalitis: a new entity? Neurosci Lett 2006;394:5–8.

4 Bien CG, Schulze-Bonhage A, Deckert M, Urbach H, Helmstaedter C, Grunwald T, Schaller C, Elger CE: Limbic encephalitis not associated with neoplasm as a cause of temporal lobe epilepsy. Neurology 2000;55:1823–1828.

5 De Tiege X, Rozenberg F, Des Portes V, Lobut JB, Lebon P, Ponsot G, Heron B: Herpes simplex encephalitis relapses in children: differentiation of two neurologic entities. Neurology 2003;61:241–243.

ABSTRACT: β-Synemin has been identified as an α-dystrobrevin–interacting protein in human muscle, although at least two synemin transcripts are expressed in brain. To understand synemin's function in neural tissue, in situ and immunohistochemical analyses were performed to identify where α- and β-synemin are expressed in the brain of C57BL/6 and *mdx* (dystrophin null) mice. This analysis shows that the α- and β-synemin transcripts and their encoded proteins colocalize in neurons, especially in the midbrain and pons. Since α-dystrobrevin-1 and synemin do not colocalize in brain as in muscle, this suggests that another member of the dystrophin-associated protein complex might interact with synemin in brain. In support of this, synemin mRNA expression was decreased in *mdx* mice, suggesting that synemin transcription is linked to dystrophin expression. Our findings show where synemin is expressed in brain and allow one to speculate with regard to its function in neural tissue.
Muscle Nerve 36: 497–504, 2007

SYNEMIN EXPRESSION IN BRAIN

YUJI MIZUNO, MD, PhD,[1] JEFFREY R. GUYON, PhD,[2] KOICHI OKAMOTO, MD, PhD,[1] and LOUIS M. KUNKEL, PhD[2]

[1] Department of Neurology, Gunma University Graduate School of Medicine, 3-39-22 Showa, Maebashi, Gunma 371-8511, Japan
[2] Howard Hughes Medical Institute/Division of Genetics, Children's Hospital Boston and Harvard Medical School, Boston, Massachusetts, USA

Accepted 11 May 2007

β-Synemin,[10,21] a novel intermediate filament protein, was originally identified as an α-dystrobrevin–binding protein through a yeast two-hybrid screen using an amino acid sequence derived from exons 1 through 16 of α-dystrobrevin,[16,17] a region common to both α-dystrobrevin-1 and -2.[10] Although this region is shared between both α-dystrobrevin isoforms, β-synemin preferentially associates with α-dystrobrevin-1 in muscle.[12] Based on its expression pattern and location in muscle, it has been postulated that β-synemin predominantly functions in muscle to maintain costameric linkages, although expression has also been observed in muscle neuromuscular junctions,[12] suggesting a role for β-synemin in transmitting neural signals to the muscles.

Although Northern blot analysis shows that a single isoform of human synemin is strongly expressed in skeletal muscle and heart, a longer exposure of the same Northern blot shows a faint doublet in brain, suggesting that there are two synemin isoforms expressed in brain tissue.[10] Both synemin isoforms derive from differential splicing of the synemin gene on chromosome 15q26.3.[11] The α-synemin transcript is larger than β-synemin's transcript, as the intron between exons 4 and 5 is not removed.[11,21] As a result, the human α-synemin protein is 312 amino acids longer at the C-terminus than β-synemin. Previous studies have shown that β-synemin is specifically expressed in skeletal muscle, whereas α- and β-synemin are expressed in brain tissue.[6,12] It is not understood why two synemin isoforms are expressed in brain, although α-synemin expression is tissue-specific, suggesting that the two proteins have different functions.

During rat brain development, synemin is expressed only in a subpopulation of astrocytic precursors that are glial fibrillary acidic protein (GFAP) and vimentin positive.[20] In the adult rat, astrocytes no longer express synemin in the cerebral hemispheres except in intermingled vascular smooth muscle cells.[20] In contrast, only the α-synemin isoform is detected in sections from normal human brain, although astrocytic tumors express both α- and β-synemin.[7] Furthermore, the α-synemin protein is highly expressed in astrocytomas compared to expression in unaffected brain.[7] Increased synemin expression in astrocytomas is likely a result of increased vascularization within the tumor and the increased numbers of reactive astrocytes.[7]

Abbreviations: EDTA, ethylenediamine tetraacetic acid; GFAP, glial fibrillary acidic protein; PBS, phosphate-buffered saline; TBS, Tris-buffered saline
Key words: α-dystrobrevin; β-synemin; desmuslin; midbrain; pons
Correspondence to: Y. Mizuno; e-mail: mizunoy@med.gunma-u.ac.jp

Published online 24 July 2007 in Wiley InterScience (www.interscience.wiley.com). DOI 10.1002/mus.20847

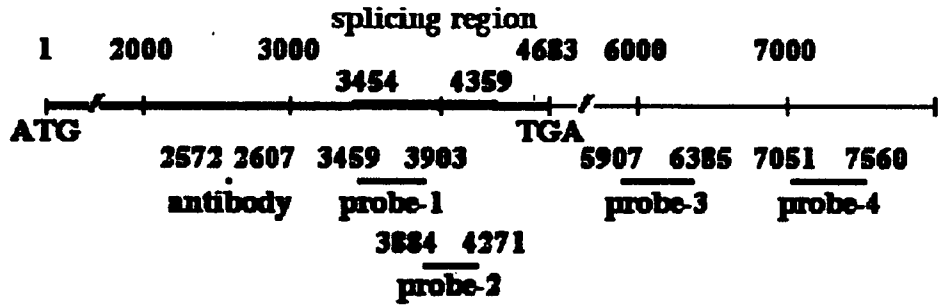

FIGURE 1. Summary of synemin, probes, and antibody. The α-synemin gene is labeled with the positions of the in situ probes and antibody-binding site. The region specific to α-synemin but spliced away in β-synemin is designated in red. Binding sites for in situ probe-1 and -2 are within the spliced region and therefore specific to α-synemin, whereas those for probe-3 and -4 are present in a noncoding region and recognize both synemin isoforms.

Since it is unknown how synemin functions in neural tissue, in situ and immunohistochemical analyses were completed to identify where the synemin transcripts and proteins are normally expressed in brain tissue. To complete this study we examined brain tissue from 8-week-old C57BL/6 mice. Sections from brain were analyzed using a human synemin antibody, which recognizes both the α- and β-synemin proteins, and four different RNA probes, two of which are located in the alternative splicing region specific to α-synemin and two of which are present in a noncoding region common to both synemin isoforms.

MATERIALS AND METHODS

RNA Probe Design and Preparation. The following four in situ probes were used in this study (Fig. 1): RNA probe-1 [445 bp; position 3524–3968 (3459–3903 bp from the initiation codon)], RNA probe-2 [388 bp; position 3949–4336 (3884–4271 bp from the initiation codon)], RNA probe-3 [479 bp; position 5972–6450 (5907–6385 bp from the initiation codon)], and RNA probe-4 [510 bp; position 7116–7625 (7051–7560 bp from the initiation codon)]. Positions are relative to the mouse muscle cDNA for synemin (GenBank access. no. NM_201639). Each gene fragment was subcloned into the pGEM-T vector (Promega, Madison, Wisconsin) and digoxigenin-RNA probes were expressed from T7 and S6 promoters to generate both the sense and anti-sense RNA probes (Roche, Basel, Switzerland).

In Situ Hybridization. All in situ hybridization protocols were performed by Genostaff (Tokyo, Japan) and all results were confirmed by repeating the experiments either two (probes-1–3) or three (probe-4) times. Mouse brains were isolated from 8-week-old C57BL/6 and *mdx* (dystrophin-deficient) mice, fixed with tissue fixative, and subsequently embedded in paraffin blocks. Dystrophic (*mdx*) mice were provided by the Central Institute for Experimental Animals (Kanagawa, Japan). Tissue sections (6 μm) were prepared for in situ hybridization. They were dewaxed with xylene and rehydrated through a series of washes with ethanol and phosphate-buffered saline (PBS). Sections were fixed in PBS with 4% paraformaldehyde for 15 min and then washed with PBS. Sections were then treated with 10 μg/ml proteinase K in PBS for 30 min at 37°C, washed with PBS, refixed with 4% paraformaldehyde in PBS, washed again with PBS, and placed in 0.2 M HCl for 10 min. After washing with PBS the sections were acetylated by incubation in 0.1 M triethanolamine-HCl (pH 8.0), 0.25% acetic anhydride for 10 min. The sections were then washed with PBS and dehydrated through a series of ethanol washes. Hybridization was performed with either RNA probe-1, -2, -3, or -4 as indicated in the text at concentrations of 100 ng/ml in probe diluent at 60°C for 16 h. After hybridization, the sections were washed in 5 × HybriWash (Genostaff, Tokyo, Japan) at 60°C for 20 min and then in 50% formamide, 2 × HybriWash at 60°C for 20 min, followed by RNase treatment in 50 μg/ml RNaseA in 10 mM Tris-HCl (pH 8.0), 1 M NaCl, and 1 mM ethylenediamine tetraacetic acid (EDTA) for 30 min at 37°C. The sections were then washed twice with 2 × HybriWash at 60°C for 20 min, twice 0.2 × HybriWash at 60°C for 20 min, and once with TBST [0.1% Tween20 in Tris-buffered saline (TBS)]. After treatment with 0.5% blocking reagent (Roche, Basel, Switzerland) in TBST for 30 min the sections were incubated with anti-digoxigenin-AP conjugate (Roche) diluted 1:1,000 with TBST for 2 h. The sections were washed twice with TBST and then incubated in 100 mM NaCl, 50 mM $MgCl_2$, 0.1% Tween20, 100 mM Tris-HCl (pH 9.5). Coloring

reactions were performed with BM purple AP substrate (Roche) overnight and then washed with PBS. The sections were counterstained with Kernechtrot stain solution (Muto Pure Chemicals, Tokyo, Japan), dehydrated, and mounted with malinol (Muto).

Immunohistochemistry. For immunohistochemistry, tissue sections were dewaxed with xylene, and rehydrated through a series of ethanol and TBS washes. Antigen retrieval was performed by microwaving the samples for 20 min with citrate buffer (pH 6.0). The sections were treated with 3% hydrogen peroxide in methanol for 15 min, and then Protein Block (Dako, Kyoto, Japan) for 10 min. The sections were treated with antihuman synemin rabbit polyclonal antibody[12] at a final concentration of 0.4 μg/ml, at 2–8°C overnight. The 12 amino acid peptide sequence used to generate the antihuman synemin antibody is conserved in mice (amino acids 857–868 in human and 848–859 in mouse). The sections were treated with Histofine Simplestain mouse MAX-PO (R) (Nichirei Biosciences, Tokyo, Japan) for 30 min, and then incubated with 3,3'-diaminobenzidine tetrahydrochloride (Wako Pure Chemical Industries, Osaka, Japan). The sections were counterstained with Mayer's hematoxylin (Muto), dehydrated, and mounted with malinol (Muto).

RESULTS

Localization of the Synemin Transcript in Mouse Midbrain, Pons, Hippocampus, and Septum. In order to investigate synemin expression in the brain, in situ analysis was performed on sagittal sections of mouse brain using a general synemin probe (see probe-3, Fig. 1). This analysis showed that synemin transcription was largely localized to the ventral side of the cerebellum (see square, Fig. 2A). Larger magnification of the same area showed more obvious staining scattered at the midbrain to pons region (Fig. 2B), and even further magnification of the square in Figure 2B (see Fig. 2C) makes it possible to discern large clear reactive neurons. As expected, the second general synemin probe (probe-4) showed a similarly labeling pattern (Fig. 2D) to that of probe-3 (Fig. 2C). In order to investigate which synemin isoform was expressed in these tissues, α-synemin specific probes (-1 and -2, Fig. 1) were used for in situ analysis in the same sagittal sections. Both probe-1 and -2 (Fig. 2E,F) in general showed similar labeling patterns as that for the general synemin probes, although the intensities were weak compared to probe-3 (Fig. 2C) and -4 (Fig. 2D). Control experiments using sense probes were negative, suggesting the labeling patterns for the antisense probes were specific (data not shown). To better illustrate the parts of the brain being analyzed, a figure from the mouse brain atlas is shown[13] with brain areas labeled (Fig. 2G).

Synemin expression was also analyzed in other brain regions. Detailed examination of the region of square-1 of Figure 3A and its corresponding region in Fig. 3B identified cells labeled by probe-3 in the septum (Fig. 3E) similar to that seen in serial sections stained with probe-1 (Fig. 3C) and -2 (Fig. 3D), although the levels of intensity with probe-3 were greater. In the dentate gyrus of the hippocampus (square-2 in Fig. 3A and its corresponding region in Fig. 3F), no cells stained with probe-1 (Fig. 3G) and only one cell staining with probe-2 was detected (Fig. 3H). Scattered cells stained by probe-3 were observed in the dentate gyrus (Fig. 3I); however, the number of positive cells was low and the intensities were weak compared to the staining observed in the midbrain and pons. The synemin-positive cells seemed to position outside of the dentate gyrus rather than inside of it. In coronal sections it was possible to identify cells stained by all four probes in the CA3 field of the hippocampus (data not shown). Based on sagittal brain sections hybridized with synemin-specific probes, detectable levels of synemin mRNA are observed in the mouse brain between the pons and midbrain, the hippocampus, and the septum.

Colocalization of the Synemin Transcript and Protein in Brain. To determine whether synemin is expressed as protein in cells expressing the synemin transcript, we examined mirror sections (sections on either side of an initial cut) of mouse brain using both in situ hybridization (using probe-3) and immunohistochemistry (using an antisynemin antibody). Mirror sections were used to determine colocalization since they provide the greatest resolution when positively labeled structures are small. In mirror sagittal sections, regions 1, 2, and 3 (Fig. 4A) demonstrated convincing colocalization of transcript and its protein. A more detailed alignment of transcript-positive (Fig. 4B,F) and protein-positive (Fig. 4C,G) structures were observed in the midbrain and pons. Higher-resolution analysis of the squares shown in Figure 4B,C,F,G demonstrated that there were large numbers of the neurons expressing both the synemin transcript (Fig. 4D,H) and its protein (Fig. 4E,I). The differences in size of the neurons are likely due to the angle at which individual neurons were sectioned (Fig. 4D,E). In the hippocampus, synemin-positive structures were very small, making them difficult to observe; however, large magnification of squares in Figure 4J,K showed that the same cells were positive with the in situ probe-3 (arrow in Fig. 4L) and the antisynemin antibody (arrow in Fig. 4M). In the

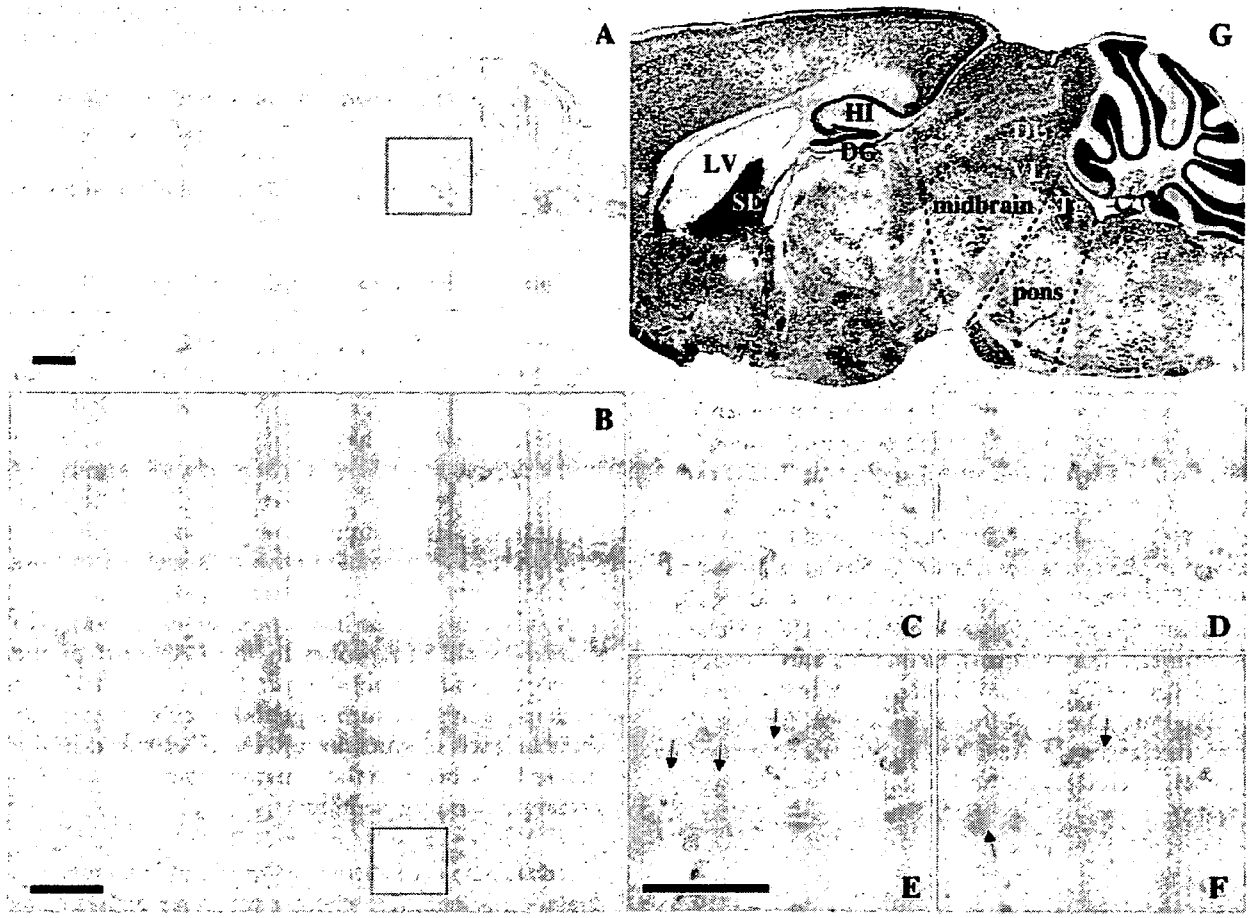

FIGURE 2. Synemin is expressed in neurons of the midbrain and pons. Sagittal sections from an 8-week-old mouse brain were examined by in situ analysis using the probes designated below. Light purple shows in situ positive structures. **(A–C)** Hybridized with probe-3; **(D)** was hybridized with probe-4; **(E,F)** were hybridized by probe-1 and probe-2, respectively. The square in **A** corresponds to **B** and shows probe-3 positive neurons from midbrain to pons. The square in **B** is further magnified and shown in **C** to better show synemin expression in neurons, similar to that shown for probe-4 **(D)**. **(E,F)** The same area as in **C,D**, yet hybridized with probe-1 and -2, respectively. Arrows indicate transcript-positive neurons. **(G)** Taken from a mouse atlas[13] and regions of the brain were labeled with regard to these analyses. DL, L, and VL indicate dorsolateral, lateral, and ventrolateral periaqueductal gray matter of midbrain, respectively, and Tg indicates laterodorsal tegmental nucleus of the pons. Other abbreviations: HI, DG, SE, and LV show hippocampus, dentate gyrus, septum, and lateral ventricle, respectively. Scale bar, 50 μm.

septum cells stained with probe-3 or the antisynemin antibody, although it was difficult to confirm colocalization even under large magnification (data not shown). Similar results were also obtained using the other general synemin in situ probe-4, and results from both probes were performed twice, confirming the specificity of our results.

Synemin Expression in Dystrophin-Deficient (*mdx*) Mice Brain. To determine whether synemin expression was altered in dystrophin-deficient mouse brain, in situ hybridizations (using probe-3) and immunohistochemical analyses (using an antisynemin antibody) were performed simultaneously on control and *mdx* mouse brain sections. In control brain synemin transcript was clearly expressed in the neurons of the midbrain to pons (Fig. 5A), while synemin expression was decreased in the *mdx* brain (Fig. 5C), suggesting that synemin mRNA expression is at least partially dependent on full-length dystrophin expression. In control mice, immunohistochemical analysis of mirror sections (Fig. 5B) shows that the synemin protein was expressed in the same neurons where synemin transcript was detected using in situ analysis (Fig. 5A). Unexpectedly, immunohistochemical analysis shows that the synemin protein was also expressed in *mdx* mice brain (Fig. 5D), even though in situ analysis detected an overall decrease in synemin mRNA levels (Fig. 5C).

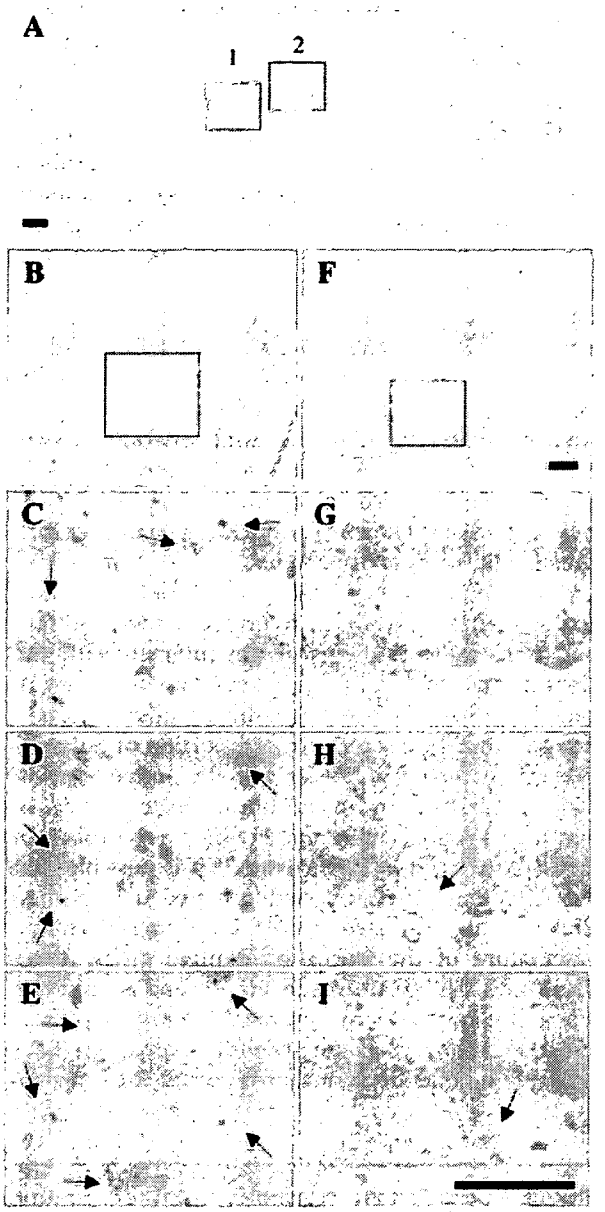

FIGURE 3. Synemin is expressed in neurons or cells of the septum and dentate gyrus. Sagittal sections from an 8-week-old mouse brain were examined by in situ analysis using the probes designated below. Light purple shows in situ positive structures. **(B,F)** The panels for squares 1 and 2 in **(A)** are shown for comparison. **(A,B,E,F,I)** Hybridized with probe-3, whereas **(C,G)** or **(D,H)** were hybridized with probe-1 or -2, respectively. The squares in **B** and **F** are shown in **E** and **I**, respectively, at a large magnification, indicating transcript-positive structures in septum and hippocampus. **(C,D)** Similar staining pattern to that shown in **E**; however, the staining intensities for **C** and **D** are weak. Both the intensity and number of synemin transcript-positive structures in dentate gyrus were very low, as shown in **G–I**. Scale bar, 50 μm.

DISCUSSION

Both mouse α- and β-synemin isoforms[22] are structurally identical to their human orthologs[10,21] with the exception that intron 4 of β-synemin is 906-bp long in mice and 936 bp in humans. In addition, a third synemin isoform exists in mice and this isoform skips exon 4 of β-synemin, thereby connecting exon 3 to exon 5, which, as a result of a frameshift, encodes a unique 36-amino acid C-terminus.[22] Previous studies have investigated the function of synemin in muscle and have shown that this protein positions to the muscle costamere (the region that connects the plasma membrane to the muscle Z-line) and to neuromuscular and myotendinous junctions.[12] These locations suggest that synemin functions in skeletal muscle as a structural protein maintaining muscle cell integrity during repeated cycles of contraction. In addition to its expression in muscle, synemin is also expressed in brain.[4,6,7,12,20] In this study, we localize the synemin transcript and its protein in mouse brain to begin understanding the characteristics of this protein in neural tissue.

Sultana et al.[20] previously reported that synemin is expressed transiently in radial glial cells, which develop into mature astrocytes in the rat brain cortex during development. Furthermore, Hirako et al.[4] showed that synemin is expressed in astrocytes of the central nervous system (such as adult bovine and rabbit optic nerve) and in non–myelin-forming Schwann cells of the peripheral nervous system. Although synemin is expressed in some astrocytes, it is not expressed in all of them. For example, tissues from progressive multifocal leukoencephalopathy and from glial scars following stroke showed synemin-positive reactive astrocytes, whereas those from epileptic foci were synemin negative.[7] Since the brain tissues we examined were from normal mice, no reactive astrocytes were likely to be found and therefore our results describe synemin expression in an unaffected system. Our results show that synemin expression is limited to neurons or cells in very restricted regions, with the strongest expression in the midbrain and pons, suggesting a role for synemin in those tissues. A mouse brain atlas shows that synemin-positive structures align in the dorsolateral, lateral, and ventrolateral periaqueductal gray of the midbrain or the laterodorsal tegmental nucleus of pons.[13] This pattern of expression suggests that synemin is expressed in some of the cranial nerves.

In mammalian muscle, both α-synemin and β-synemin are incorporated with desmin into heteropolymeric intermediate filaments.[4] Whether synemin in the midbrain and pons colocalizes with

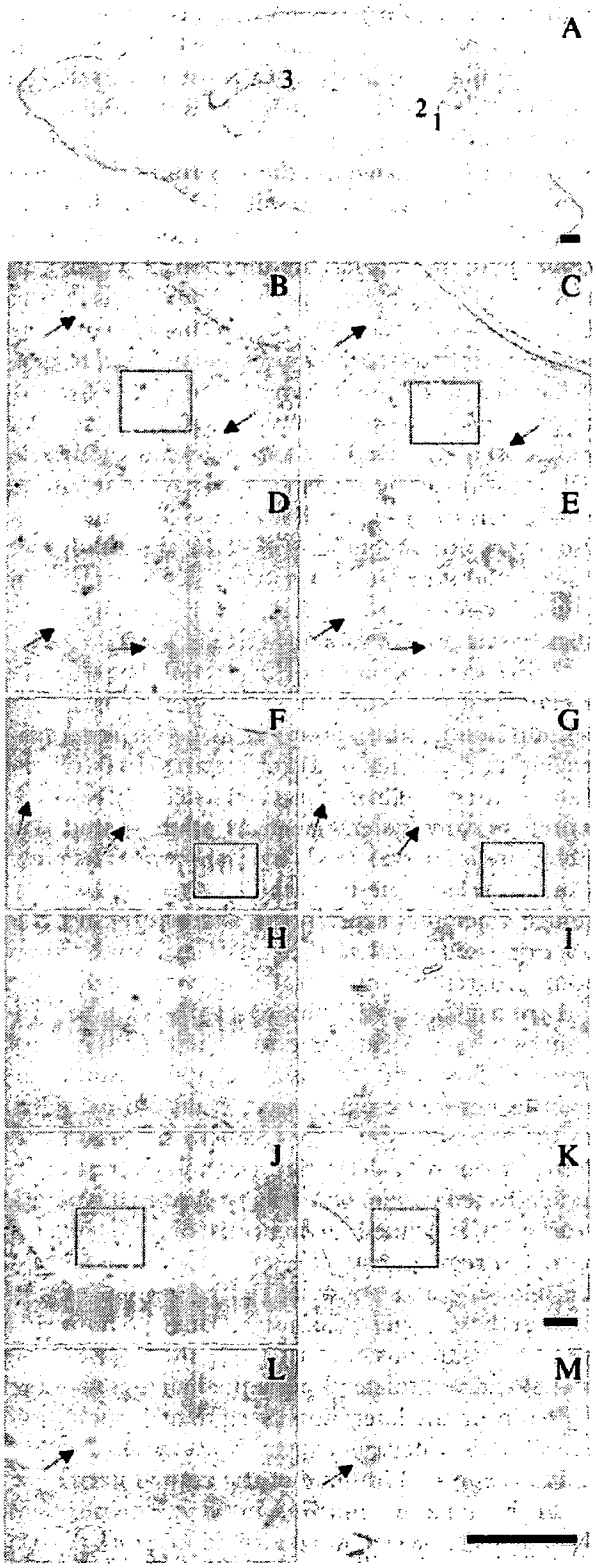

other intermediate filament proteins or dimerizes with another synemin isoform is not understood. Given that β-synemin is a smaller splice variant of α-synemin, it is impossible to generate a probe specific to the β-isoform. Although synemin expression patterns were very similar using probe-1 and probe-2 (specific to α-synemin) and probe-3 and probe-4 (common to both synemin transcripts), the intensities of the reactions were different, suggesting that β-synemin dimerizes with α-synemin in different molar ratios. In addition, since astrocytes in optic nerves and non–myelin-forming Schwann cells show synemin, GFAP and vimentin-positive reactions and astrocytes of rabbit spinal cord lack synemin but are GFAP-positive,[4] it would be helpful to understand what proteins might interact with synemin in vivo. Based on its role in skeletal muscle, synemin likely plays a role in maintaining mechanical integrity of neural cells and tissues by connecting type III and IV intermediate filament proteins.

It is tempting to speculate why synemin is most strongly expressed in the neurons of the midbrain and pons and whether synemin interacts with the dystrophin-associated proteins in brain as it does in muscle. β-Synemin was originally identified through a yeast two-hybrid screen using a portion of α-dystrobrevin as the "bait."[10] In muscle, α-dystrobrevin binds to dystrophin on the intracellular portion of the sarcolemmal membrane.[18] Since α-dystrobrevin is also expressed in brain tissue,[16] it is possible that this interaction is maintained in brain. According to Blake et al.,[1] α-dystrobrevin-1 is expressed in the vasculature of the isocortex, dentate gyrus, astrocytes, and CA2/CA3 in the hippocampus, and the soma and processes of Bergmann astroglial cells in the cerebellum. Because synemin expression does not always coincide with that reported for α-dystro-

FIGURE 4. Colocalization of the synemin transcript and protein in mouse sagittal brain. **(B,D,F,H,J,L)** In situ experiments hybridized with probe-3, whereas **(C,E,G,I,K,M)** are mirror sections immunostained with an antisynemin antibody. Light purple shows in situ positive structures and orange indicates those immunostained with the antibody. The location of the pons is designated with a "1" in **(A)** and its respective staining patterns are shown in **(B–E)**. The squares in **B** and **C** are shown in **D** and **E**, respectively, and show clear colocalization of the synemin transcript and protein. The location of midbrain is designated with a "2" in **A** and its respective staining patterns are shown in **F–I**. The squares in **F** and **G** are shown in **H** and **I**, respectively. The CA3 field of hippocampus is designated with a "3" in **A** and its respective staining patterns are shown in **J–M**. The squares in **J** and **K** are shown in **L** and **M**. Arrows indicate structures positively staining with both the in situ probe and the anti-synemin antibody. Scale bar, 50 μm.

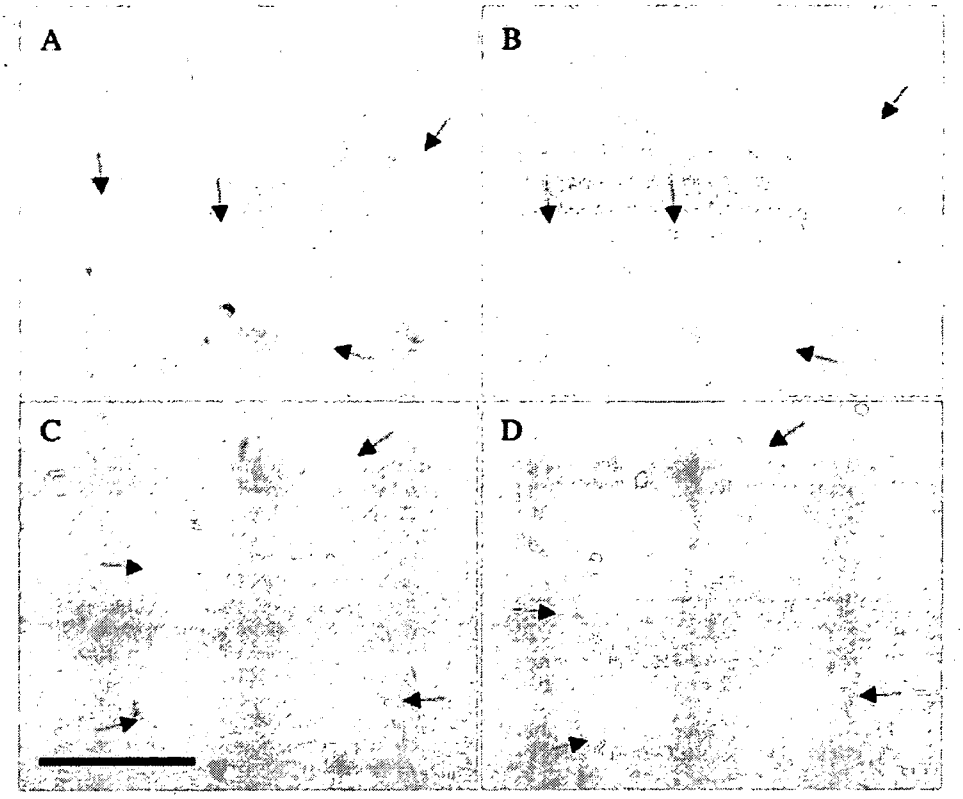

FIGURE 5. Synemin expression in control and dystrophin-deficient (*mdx*) mouse brain. **(A,C)** In situ experiments hybridized with synemin probe-3, whereas **(B,D)** are mirror sections immunostained with an anti-synemin antibody. **A** and **B** are from control mice, whereas **C** and **D** are from *mdx* mice. Light purple shows in situ positive structures and orange indicates those immunostained with the antibody. Arrows indicate structures positively stained with both the in situ probe-3 and the antisynemin antibody. Scale bar, 50 μm.

brevin-1 in brain, it is likely that synemin forms a different complex in brain from that observed in skeletal muscle. Furthermore, β-dystrobrevin,[14,15] a second member of the dystrobrevin family, is expressed predominantly in granule cells and Purkinje cell somata in the cerebellum, a region where synemin was not expressed, suggesting that β-synemin also does not colocalize with β-dystrobrevin in brain. Using an immunohistochemical analysis, Izmiryan et al.[6] recently reported the expression of α- and β-synemin in Purkinje cells in mouse adult brain. In addition, they reported synemin expression in the medulla oblongata, but not in the midbrain or pons. Since our study evaluated synemin expression at both the mRNA and protein levels, we cannot fully explain the differences with their immunohistochemical data, although this could be caused by varying specificities of the two different antibodies used in these studies.

In muscle, synemin is connected to dystrophin through its association with α-dystrobrevin and it is possible that the connection between synemin and dystrophin is maintained either directly or indirectly in brain tissue. To determine whether dystrophin expression is required for synemin localization in brain, in situ analysis was performed for synemin in normal and dystrophic (*mdx*) mouse brain. Synemin mRNA levels were decreased in the brain of *mdx* mice (Fig. 5A,C), suggesting that changes in dystrophin expression affect synemin mRNA expression. Unexpectedly, though, the synemin protein did not show the same decrease in expression levels as its mRNA transcript (Fig. 5B,D). There are at least two possible explanations for this observation. First, since the causative dystrophin point mutation[19] in *mdx* mice is upstream of the initiation codon for the smaller dystrophin isoforms (<260 kDa),[1-3,5,8,9] it is possible that the dystrophin-short isoforms were able to stabilize the synemin protein in the *mdx* brain tissue. Second, it is also possible that the antibody used in this study recognizes synemin along with another related protein although previous antibody characterization does not support this explanation.[12]

In summary, we have identified regions where synemin is expressed in the adult mouse brain. These results show that synemin transcript and pro-